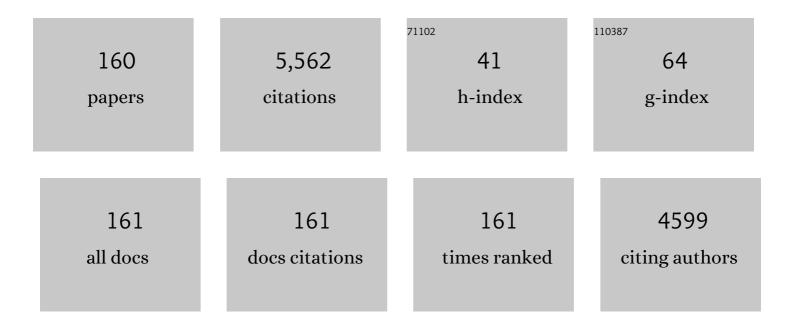
List of Publications by Year in descending order

Source: https://exaly.com/author-pdf/6351683/publications.pdf Version: 2024-02-01



#	Article	IF	CITATIONS
1	Geometry and flow in ascending aortic aneurysms are influenced by left ventricular outflow tract orientation: Detecting increased wall shear stress on the outer curve of proximal aortic aneurysms. Journal of Thoracic and Cardiovascular Surgery, 2023, 166, 11-21.e1.	0.8	6
2	Evaluation and verification of patient-specific modelling of type B aortic dissection. Computers in Biology and Medicine, 2022, 140, 105053.	7.0	14
3	Multiphysics Modelling and Simulation of Thrombolysis via Activated Platelet-Targeted Nanomedicine. Pharmaceutical Research, 2022, 39, 41-56.	3.5	3
4	An integrated fluid–structure interaction and thrombosis model for type B aortic dissection. Biomechanics and Modeling in Mechanobiology, 2022, 21, 261-275.	2.8	9
5	Haemodynamic Analysis of Branched Endografts for Complex Aortic Arch Repair. Bioengineering, 2022, 9, 45.	3.5	6
6	Prediction of aortic dilatation in surgically repaired type A dissection: A longitudinal study using computational fluid dynamics. JTCVS Open, 2022, 9, 11-27.	0.5	9
7	Evaluation of Computational Methodologies for Accurate Prediction of Wall Shear Stress and Turbulence Parameters in a Patient-Specific Aorta. Frontiers in Bioengineering and Biotechnology, 2022, 10, 836611.	4.1	10
8	The Haemodynamic and Pathophysiological Mechanisms of Calcific Aortic Valve Disease. Biomedicines, 2022, 10, 1317.	3.2	1
9	Computational Modeling of Flow and Thrombus Formation in Type B Aortic Dissection: The Influence of False Lumen Perfused Side Branches. Studies in Mechanobiology, Tissue Engineering and Biomaterials, 2022, , 53-72.	1.0	7
10	The influence of inlet velocity profile on predicted flow in type B aortic dissection. Biomechanics and Modeling in Mechanobiology, 2021, 20, 481-490.	2.8	40
11	MR-labelled liposomes and focused ultrasound for spatiotemporally controlled drug release in triple negative breast cancers in mice. Nanotheranostics, 2021, 5, 125-142.	5.2	18
12	Analysis of Turbulence Effects in a Patient-Specific Aorta with Aortic Valve Stenosis. Cardiovascular Engineering and Technology, 2021, 12, 438-453.	1.6	29
13	Correlations for Concentration Polarization and Pressure Drop in Spacer-Filled RO Membrane Modules Based on CFD Simulations. Membranes, 2021, 11, 338.	3.0	14
14	Effect of Vessel Tortuosity on Stress Concentration at the Distal Stent–Vessel Interface: Possible Link With New Entry Formation Through Biomechanical Simulation. Journal of Biomechanical Engineering, 2021, 143, .	1.3	6
15	Association of hemodynamic factors and progressive aortic dilatation following type A aortic dissection surgical repair. Scientific Reports, 2021, 11, 11521.	3.3	15
16	Fibrinogen-mimicking, multiarm nanovesicles for human thrombus-specific delivery of tissue plasminogen activator and targeted thrombolytic therapy. Science Advances, 2021, 7, .	10.3	33
17	Patient-Specific Virtual Stent-Graft Deployment for Type B Aortic Dissection: A Pilot Study of the Impact of Stent-Graft Length. Frontiers in Physiology, 2021, 12, 718140.	2.8	17
18	Patient-specific simulation of stent-graft deployment in type B aortic dissection: model development and validation. Biomechanics and Modeling in Mechanobiology, 2021, 20, 2247-2258.	2.8	17

#	Article	IF	CITATIONS
19	Qualitative and Quantitative Assessments of Blood Flow on Tears in Type B Aortic Dissection With Different Morphologies. Frontiers in Bioengineering and Biotechnology, 2021, 9, 742985.	4.1	6
20	High Wall Shear Stress can Predict Wall Degradation in Ascending Aortic Aneurysms: An Integrated Biomechanics Study. Frontiers in Bioengineering and Biotechnology, 2021, 9, 750656.	4.1	28
21	Modelling Combined Intravenous Thrombolysis and Mechanical Thrombectomy in Acute Ischaemic Stroke: Understanding the Relationship between Stent Retriever Configuration and Clot Lysis Mechanisms. Life, 2021, 11, 1271.	2.4	4
22	Abstract 10478: Comprehensive Mechanical Modelling of Thoracic Endovascular Aortic Repair in Type A Aortic Dissection. Circulation, 2021, 144, .	1.6	1
23	Phase-contrast magnetic resonance imaging and computational fluid dynamics assessment of thoracic aorta blood flow: a literature review. European Journal of Cardio-thoracic Surgery, 2020, 57, 438-446.	1.4	5
24	Finite element modeling to predict procedural success of thoracic endovascular aortic repair in type A aortic dissection. JTCVS Techniques, 2020, 4, 40-47.	0.4	13
25	Effect of intimal flap motion on flow in acute type B aortic dissection by using fluidâ€structure interaction. International Journal for Numerical Methods in Biomedical Engineering, 2020, 36, e3399.	2.1	14
26	The effect of turbulence on transitional flow in the <scp>FDA</scp> 's benchmark nozzle model using largeâ€eddy simulation. International Journal for Numerical Methods in Biomedical Engineering, 2020, 36, e3389.	2.1	13
27	Location of Reentry Tears Affects False Lumen Thrombosis in Aortic Dissection Following TEVAR. Journal of Endovascular Therapy, 2020, 27, 396-404.	1.5	26
28	A combined experimental and computational study of the flow characteristics in a Type B aortic dissection: Effect of primary and secondary tear size. Chemical Engineering Research and Design, 2020, 160, 240-253.	5.6	17
29	A Computational Study of the Effect of Stent Design on Local Hemodynamic Factors at the Carotid Artery Bifurcation. Artery Research, 2020, 26, 161-169.	0.6	9
30	Dissection Level Within Aortic Wall Layers is Associated with Propagation of Type B Aortic Dissection: A Swine Model Study. European Journal of Vascular and Endovascular Surgery, 2019, 58, 415-425.	1.5	9
31	Evaluation of 4D flow MRI-based non-invasive pressure assessment in aortic coarctations. Journal of Biomechanics, 2019, 94, 13-21.	2.1	35
32	Computational simulations of thrombolysis in acute stroke: Effect of clot size and location on recanalisation. Medical Engineering and Physics, 2019, 73, 9-17.	1.7	10
33	Pore-scale direct numerical simulation of particle transport in porous media. Chemical Engineering Science, 2019, 199, 613-627.	3.8	50
34	Towards a multiphysics modelling framework for thermosensitive liposomal drug delivery to solid tumour combined with focused ultrasound hyperthermia. Biophysics Reports, 2019, 5, 43-59.	0.8	31
35	4-D Flow MRI-Based Computational Analysis of Blood Flow in Patient-Specific Aortic Dissection. IEEE Transactions on Biomedical Engineering, 2019, 66, 3411-3419.	4.2	48
36	Mathematical Modelling of Intravenous Thrombolysis in Acute Ischaemic stroke: Effects of Dose Regimens on Levels of Fibrinolytic Proteins and Clot Lysis Time. Pharmaceutics, 2019, 11, 111.	4.5	15

#	Article	IF	CITATIONS
37	An activated-platelet-sensitive nanocarrier enables targeted delivery of tissue plasminogen activator for effective thrombolytic therapy. Journal of Controlled Release, 2019, 300, 1-12.	9.9	61
38	A pilot study of aortic hemodynamics before and after thoracic endovascular repair with a double-branched endograft. Medicine in Novel Technology and Devices, 2019, 4, 100027.	1.6	10
39	Disturbed Flow in a Stenosed Carotid Artery Bifurcation: Comparison of RANS-Based Transitional Model and LES with Experimental Measurements. International Journal of Applied Mechanics, 2019, 11, 1950032.	2.2	17
40	Thermosensitive Liposome-Mediated Drug Delivery in Chemotherapy: Mathematical Modelling for Spatio–temporal Drug Distribution and Model-Based Optimisation. Pharmaceutics, 2019, 11, 637.	4.5	10
41	Aortic Leaflet Stress in Surgery for Genetically Determined Root Aneurysms: Biomechanical Insights. Annals of Thoracic Surgery, 2018, 105, 984.	1.3	1
42	Hemodynamic evaluation using four-dimensional flow magnetic resonance imaging for a patient with multichanneled aortic dissection. Journal of Vascular Surgery Cases and Innovative Techniques, 2018, 4, 67-71.	0.6	7
43	Image-guided thermosensitive liposomes for focused ultrasound drug delivery: Using NIRF-labelled lipids and topotecan to visualise the effects of hyperthermia in tumours. Journal of Controlled Release, 2018, 280, 87-98.	9.9	66
44	Computational study of aortic hemodynamics for patients with an abnormal aortic valve: The importance of secondary flow at the ascending aorta inlet. APL Bioengineering, 2018, 2, 026101.	6.2	44
45	Incidence and risk factors for retrograde type A dissection and stent graft-induced new entry after thoracic endovascular aortic repair. Journal of Vascular Surgery, 2018, 67, 1026-1033.e2.	1.1	101
46	A computational model for false lumen thrombosis in type B aortic dissection following thoracic endovascular repair. Journal of Biomechanics, 2018, 66, 36-43.	2.1	46
47	Computational Simulations of Thrombolytic Therapy in Acute Ischaemic Stroke. Scientific Reports, 2018, 8, 15810.	3.3	30
48	3D-Bioprinting and Micro-/Nano-Technology: Emerging Technologies in Biomedical Sciences. Advanced Drug Delivery Reviews, 2018, 132, 1-2.	13.7	1
49	High Wall Stress May Predict the Formation of Stent-Graft–Induced New Entries After Thoracic Endovascular Aortic Repair. Journal of Endovascular Therapy, 2018, 25, 571-577.	1.5	23
50	Computational modelling of drug delivery to solid tumour: Understanding the interplay between chemotherapeutics and biological system for optimised delivery systems. Advanced Drug Delivery Reviews, 2018, 132, 81-103.	13.7	59
51	The effect of feed spacer geometry on membrane performance and concentration polarisation based on 3D CFD simulations. Journal of Membrane Science, 2017, 527, 78-91.	8.2	106
52	On the choice of outlet boundary conditions for patient-specific analysis of aortic flow using computational fluid dynamics. Journal of Biomechanics, 2017, 60, 15-21.	2.1	116
53	A predictive model for spiral wound reverse osmosis membrane modules: The effect of winding geometry and accurate geometric details. Computers and Chemical Engineering, 2017, 96, 248-265.	3.8	28
54	The effect of tumour size on drug transport and uptake in 3-D tumour models reconstructed from magnetic resonance images. PLoS ONE, 2017, 12, e0172276.	2.5	35

#	Article	IF	CITATIONS
55	Hemodynamic Functions of Fenestrated Stent Graft under Resting, Hypertension, and Exercise Conditions. Frontiers in Surgery, 2016, 3, 35.	1.4	4
56	Predicting false lumen thrombosis in patient-specific models of aortic dissection. Journal of the Royal Society Interface, 2016, 13, 20160759.	3.4	80
57	Effects of aortic root motion on wall stress in the Marfan aorta before and after personalised aortic root support (PEARS) surgery. Journal of Biomechanics, 2016, 49, 2076-2084.	2.1	23
58	Effect of a Flared Renal Stent on the Performance of Fenestrated Stent-Grafts at Rest and Exercise Conditions. Journal of Endovascular Therapy, 2016, 23, 809-820.	1.5	15
59	Carotid endothelial shear stress reduction with aging is associated with plaque development in twelve years. Atherosclerosis, 2016, 251, 63-69.	0.8	35
60	Mathematical modeling of thrombus formation in idealized models of aortic dissection: initial findings and potential applications. Journal of Mathematical Biology, 2016, 73, 1205-1226.	1.9	88
61	Aortic flow patterns before and after personalised external aortic root support implantation in Marfan patients. Journal of Biomechanics, 2016, 49, 100-111.	2.1	15
62	Assessment of Hemodynamic Conditions in the Aorta Following Root Replacement with Composite Valve-Conduit Graft. Annals of Biomedical Engineering, 2016, 44, 1392-1404.	2.5	17
63	Towards a multi-physics modelling framework for thrombolysis under the influence of blood flow. Journal of the Royal Society Interface, 2015, 12, 20150949.	3.4	18
64	A twoâ€layer mesh method for discrete element simulation of gasâ€particle systems with arbitrarily polyhedral mesh. International Journal for Numerical Methods in Engineering, 2015, 103, 759-780.	2.8	37
65	A viscoelastic fluid–structure interaction model for carotid arteries under pulsatile flow. International Journal for Numerical Methods in Biomedical Engineering, 2015, 31, e02709.	2.1	15
66	Biomechanical properties of the Marfan's aortic root and ascending aorta before and after personalised external aortic root support surgery. Medical Engineering and Physics, 2015, 37, 759-766.	1.7	11
67	Comparison of Blood Flow in Branched and Fenestrated Stent-Grafts for Endovascular Repair of Abdominal Aortic Aneurysms. Journal of Endovascular Therapy, 2015, 22, 578-590.	1.5	37
68	A systematic study of temperature sensitive liposomal delivery of doxorubicin using a mathematical model. Computers in Biology and Medicine, 2015, 60, 107-116.	7.0	18
69	Intrinsic and induced drug resistance mechanisms: in silico investigations at the cellular and tissue scales. Integrative Biology (United Kingdom), 2015, 7, 1044-1060.	1.3	4
70	Flow pattern analysis in a highly stenotic patient-specific carotid bifurcation model using a turbulence model. Computer Methods in Biomechanics and Biomedical Engineering, 2015, 18, 1099-1107.	1.6	22
71	Geometric and Flow Features of Type B Aortic Dissection: Initial Findings and Comparison of Medically Treated and Stented Cases. Annals of Biomedical Engineering, 2015, 43, 177-189.	2.5	64
72	Effect of heterogeneous microvasculature distribution on drug delivery to solid tumour. Journal Physics D: Applied Physics, 2014, 47, 475401.	2.8	29

#	Article	IF	CITATIONS
73	Physical characterisation and yield stress of a concentrated Miscanthus suspension. Rheologica Acta, 2014, 53, 805-815.	2.4	5
74	In-vivo assessment of the morphology and hemodynamic functions of the BioValsalvaâ,,¢ composite valve-conduit graft using cardiac magnetic resonance imaging and computational modelling technology. Journal of Cardiothoracic Surgery, 2014, 9, 193.	1.1	9
75	Towards an integrated systems-based modelling framework for drug transport and its effect on tumour cells. Journal of Biological Engineering, 2014, 8, 3.	4.7	7
76	Hemodynamic changes in the femoral vein with increasing outflow resistance. Journal of Vascular Surgery: Venous and Lymphatic Disorders, 2014, 2, 26-33.	1.6	4
77	Patient-Specific Coronary Stenoses Can Be Modeled Using a Combination of OCT and Flow Velocities to Accurately Predict Hyperemic Pressure Gradients. IEEE Transactions on Biomedical Engineering, 2014, 61, 1902-1913.	4.2	14
78	Patient-specific analysis of displacement forces acting on fenestrated stent grafts for endovascular aneurysm repair. Journal of Biomechanics, 2014, 47, 3546-3554.	2.1	32
79	Predicting flow in aortic dissection: Comparison of computational model with PC-MRI velocity measurements. Medical Engineering and Physics, 2014, 36, 1176-1184.	1.7	70
80	Coronary arterial dynamics computation with medical-image-based time-dependent anatomical models and element-based zero-stress state estimates. Computational Mechanics, 2014, 54, 1047-1053.	4.0	43
81	An improved version of RIGID for discrete element simulation of particle flows with arbitrarily complex geometries. Powder Technology, 2014, 253, 393-405.	4.2	16
82	Mathematical Modelling of Drug Transport and Uptake in a Realistic Model of Solid Tumour. Protein and Peptide Letters, 2014, 21, 1146-1156.	0.9	17
83	A novel fully automated method for mitral regurgitant orifice area quantification. International Journal of Cardiology, 2013, 166, 688-695.	1.7	7
84	Predicting Impending Rupture of the Ascending Aorta With Bicuspid Aortic Valve. JACC: Cardiovascular Imaging, 2013, 6, 1017-1019.	5.3	12
85	Finite element analysis of the deformation of deep veins in the lower limb under external compression. Medical Engineering and Physics, 2013, 35, 515-523.	1.7	14
86	Investigating the effects of ABC transporter-based acquired drug resistance mechanisms at the cellular and tissue scale. Integrative Biology (United Kingdom), 2013, 5, 555.	1.3	10
87	Evidence-based recommendations for PISA measurements in mitral regurgitation: systematic review, clinical and in-vitro study. International Journal of Cardiology, 2013, 168, 1220-1228.	1.7	19
88	Towards an understanding of the release behavior of temperature-sensitive liposomes: a possible explanation of the "pseudoequilibrium―release behavior at the phase transition temperature. Journal of Liposome Research, 2013, 23, 167-173.	3.3	10
89	A Numerical Study of Aortic Flow Stability and Comparison With In Vivo Flow Measurements. Journal of Biomechanical Engineering, 2013, 135, 011003.	1.3	44
90	A Mathematical Model for Thermosensitive Liposomal Delivery of Doxorubicin to Solid Tumour. Journal of Drug Delivery, 2013, 2013, 1-13.	2.5	42

#	Article	IF	CITATIONS
91	Assessment of Energy Requirement for the Retinal Arterial Network in Normal and Hypertensive Subjects. Journal of Biomechanical Engineering, 2012, 134, 014501.	1.3	9
92	Nitric oxide transport in an axisymmetric stenosis. Journal of the Royal Society Interface, 2012, 9, 2468-2478.	3.4	23
93	Magnetic resonance venous velocity mapping during intermittent pneumatic compression of the calf and foot. Phlebology, 2012, 27, 352-359.	1.2	3
94	Shear-induced platelet activation and its relationship with blood flow topology in a numerical model of stenosed carotid bifurcation. European Journal of Mechanics, B/Fluids, 2012, 35, 92-101.	2.5	31
95	Kissing Balloon or Sequential Dilation of the Side Branch and Main Vessel for Provisional Stenting of Bifurcations. JACC: Cardiovascular Interventions, 2012, 5, 47-56.	2.9	111
96	Simulation of ex vivo bone marrow culture: Application to chronic myeloid leukaemia growth model. Biochemical Engineering Journal, 2012, 61, 66-77.	3.6	10
97	Integrated morphologic and functional assessment of the aortic root after different tissue valve root replacement procedures. Journal of Thoracic and Cardiovascular Surgery, 2012, 143, 1422-1428.e2.	0.8	38
98	Analysis of flow and wall shear stress in the peroneal veins under external compression based on real-time MR images. Medical Engineering and Physics, 2012, 34, 17-27.	1.7	14
99	Comparison of Aortic Flow Patterns Before and After Transcatheter Aortic Valve Implantation. Cardiovascular Engineering and Technology, 2012, 3, 123-135.	1.6	20
100	Comparison of LES of Steady Transitional Flow in an Idealized Stenosed Axisymmetric Artery Model With a RANS Transitional Model. Journal of Biomechanical Engineering, 2011, 133, 051001.	1.3	40
101	Use of mathematical models to understand anticancer drug delivery and its effect on solid tumors. Pharmacogenomics, 2011, 12, 1337-1348.	1.3	16
102	Computational biomechanics of the aortic root. Aswan Heart Centre Science & Practice Series, 2011, 2011, .	0.3	6
103	Development of lysolipid-based thermosensitive liposomes for delivery of high molecular weight proteins. International Journal of Pharmaceutics, 2011, 421, 291-292.	5.2	13
104	Discrete element simulation of particle flow in arbitrarily complex geometries. Chemical Engineering Science, 2011, 66, 6069-6088.	3.8	61
105	A systems-based mathematical modelling framework for investigating the effect of drugs on solid tumours. Theoretical Biology and Medical Modelling, 2011, 8, 45.	2.1	11
106	MR phase ontrast velocity mapping methods for measuring venous blood velocity in the deep veins of the calf. Journal of Magnetic Resonance Imaging, 2011, 34, 634-644.	3.4	8
107	MR Image-Based Geometric and Hemodynamic Investigation of the Right Coronary Artery with Dynamic Vessel Motion. Annals of Biomedical Engineering, 2010, 38, 2606-2620.	2.5	42
108	High Levels of 18F-FDG Uptake in Aortic Aneurysm Wall are Associated with High Wall Stress. European Journal of Vascular and Endovascular Surgery, 2010, 39, 295-301.	1.5	90

#	Article	lF	CITATIONS
109	Introduction to the biomechanics of carotid plaque pathogenesis and rupture: review of the clinical evidence. British Journal of Radiology, 2010, 83, 729-735.	2.2	36
110	Carotid Artery Hemodynamics: Observing Patient-specific Changes with Amlodipine and Lisinopril by Using MR Imaging Computation Fluid Dynamics. Radiology, 2010, 257, 662-669.	7.3	4
111	Local fixed pivot quadratue method of moment for bubble population balance equation including coalescence and breakage. , 2010, , .		1
112	Analysis of Flow Patterns in a Patient-Specific Aortic Dissection Model. Journal of Biomechanical Engineering, 2010, 132, 051007.	1.3	111
113	Combined imaging, computational and histological analysis of a ruptured carotid plaque: A patient-specific analysis. Artery Research, 2010, 4, 59.	0.6	7
114	Computational Analysis of Oxygen Transport in the Retinal Arterial Network. Current Eye Research, 2009, 34, 945-956.	1.5	47
115	FLUID-STRUCTURE INTERACTION ANALYSIS OF WALL STRESS AND FLOW PATTERNS IN A THORACIC AORTIC ANEURYSM. International Journal of Applied Mechanics, 2009, 01, 179-199.	2.2	44
116	Computational Modeling of LDL and Albumin Transport in an In Vivo CT Image-Based Human Right Coronary Artery. Journal of Biomechanical Engineering, 2009, 131, 021003.	1.3	46
117	Computational analysis of oxygen transport in a patient-specific model of abdominal aortic aneurysm with intraluminal thrombus. British Journal of Radiology, 2009, 82, S18-S23.	2.2	26
118	Fluid–structure interaction analysis of a patientâ€specific right coronary artery with physiological velocity and pressure waveforms. Communications in Numerical Methods in Engineering, 2009, 25, 565-580.	1.3	111
119	Simulation of micro-behaviors including nucleation, growth, and aggregation in particle system. Science in China Series B: Chemistry, 2009, 52, 241-248.	0.8	9
120	Advances in numerical methods for the solution of population balance equations for disperse phase systems. Science in China Series B: Chemistry, 2009, 52, 1063-1079.	0.8	19
121	Modelling in congenital heart disease. Art or science?. International Journal of Cardiology, 2009, 133, 141-144.	1.7	4
122	Low wall shear stress predicts subsequent development of wall hypertrophy in lower limb bypass grafts. Artery Research, 2009, 3, 32.	0.6	30
123	Fluid–solid interaction simulation of flow and stress pattern in thoracoabdominal aneurysms: A patient-specific study. Journal of Fluids and Structures, 2008, 24, 270-280.	3.4	64
124	An adaptive direct quadrature method of moment for population balance equations. AICHE Journal, 2008, 54, 2872-2887.	3.6	24
125	Analysis of Flow Disturbance in a Stenosed Carotid Artery Bifurcation Using Two-Equation Transitional and Turbulence Models. Journal of Biomechanical Engineering, 2008, 130, 061008.	1.3	79
126	Effects of elastic compression stockings on wall shear stress in deep and superficial veins of the calf. American Journal of Physiology - Heart and Circulatory Physiology, 2008, 294, H2112-H2120.	3.2	44

#	Article	IF	CITATIONS
127	Effects of transmural pressure and wall shear stress on LDL accumulation in the arterial wall: a numerical study using a multilayered model. American Journal of Physiology - Heart and Circulatory Physiology, 2007, 292, H3148-H3157.	3.2	62
128	Role of MRI in investigating the effects of elastic compression stockings on the deformation of the superficial and deep veins in the lower leg. Journal of Magnetic Resonance Imaging, 2007, 26, 80-85.	3.4	22
129	Solution of population balance equation using quadrature method of moments with an adjustable factor. Chemical Engineering Science, 2007, 62, 5897-5911.	3.8	50
130	A combined fluid dynamics, mass transport and cell growth model for a three-dimensional perfused biorector for tissue engineering of haematopoietic cells. Biochemical Engineering Journal, 2007, 35, 1-11.	3.6	35
131	Influence of Pulsatile Flow on LDL Transport in the Arterial Wall. Annals of Biomedical Engineering, 2007, 35, 1782-1790.	2.5	31
132	A computational study on the influence of catheter-delivered intravascular probes on blood flow in a coronary artery model. Journal of Biomechanics, 2007, 40, 2501-2509.	2.1	22
133	Curvature and tortuosity of the superficial femoral artery: a possible risk factor for peripheral arterial disease. Journal of Applied Physiology, 2006, 101, 1412-1418.	2.5	119
134	Fluid-Wall Modelling of Mass Transfer in an Axisymmetric Stenosis: Effects of Shear-Dependent Transport Properties. Annals of Biomedical Engineering, 2006, 34, 1119-1128.	2.5	90
135	Operator dependence of 3-D ultrasound-based computational fluid dynamics for the carotid bifurcation. IEEE Transactions on Medical Imaging, 2005, 24, 451-456.	8.9	23
136	Relationship between carotid artery intima-media thickness and wall shear stress derived parameters. Computer Methods in Biomechanics and Biomedical Engineering, 2005, 8, 279-280.	1.6	7
137	APPLICATION OF ULTRASOUND-BASED COMPUTATIONAL FLUID DYNAMICS TO MODELING BLOOD FLOW IN THE CAROTID BIFURCATION. , 2005, , 109-156.		0
138	Image-based carotid flow reconstruction: a comparison between MRI and ultrasound. Physiological Measurement, 2004, 25, 1495-1509.	2.1	57
139	Ultrasound image-based computer model of a common carotid artery with a plaque. Medical Engineering and Physics, 2004, 26, 823-840.	1.7	36
140	MRI and CFD studies of pulsatile flow in healthy and stenosed carotid bifurcation models. Journal of Biomechanics, 2004, 37, 679-687.	2.1	214
141	Reproducibility Study of Magnetic Resonance Image-Based Computational Fluid Dynamics Prediction of Carotid Bifurcation Flow. Annals of Biomedical Engineering, 2003, 31, 142-151.	2.5	80
142	Comparative Study of Magnetic Resonance Imaging and Image-Based Computational Fluid Dynamics for Quantification of Pulsatile Flow in a Carotid Bifurcation Phantom. Annals of Biomedical Engineering, 2003, 31, 962-971.	2.5	47
143	Various issues relating to computational fluid dynamics simulations of carotid bifurcation flow based on models reconstructed from three-dimensional ultrasound images. Proceedings of the Institution of Mechanical Engineers, Part H: Journal of Engineering in Medicine, 2003, 217, 393-403.	1.8	23
144	Carotid geometry reconstruction: a comparison between MRI and ultrasound. Medical Physics, 2003, 30, 3251-3261.	3.0	28

#	Article	IF	CITATIONS
145	Accuracy and Reproducibility of CFD Predicted Wall Shear Stress Using 3D Ultrasound Images. Journal of Biomechanical Engineering, 2003, 125, 218-222.	1.3	56
146	The Influence of Inflow Boundary Conditions on Intra Left Ventricle Flow Predictions. Journal of Biomechanical Engineering, 2003, 125, 922-927.	1.3	53
147	Measurement of hemodynamics in human carotid artery using ultrasound and computational fluid dynamics. Journal of Applied Physiology, 2002, 92, 957-961.	2.5	18
148	Modelling of flow and wall behaviour in a mildly stenosed tube. Medical Engineering and Physics, 2002, 24, 575-586.	1.7	86
149	Inter-individual variations in wall shear stress and mechanical stress distributions at the carotid artery bifurcation of healthy humans. Journal of Biomechanics, 2002, 35, 1367-1377.	2.1	114
150	Quantification of the non-planarity of the human carotid bifurcation. Biorheology, 2002, 39, 419-24.	0.4	4
151	Quantitative comparison of CFD predicted and MRI measured velocity fields in a carotid bifurcation phantom. Biorheology, 2002, 39, 467-74.	0.4	22
152	MRI measurement of wall shear stress vectors in bifurcation models and comparison with CFD predictions. Journal of Magnetic Resonance Imaging, 2001, 14, 563-573.	3.4	76
153	Numerical investigation of physiologically realistic pulsatile flow through arterial stenosis. Journal of Biomechanics, 2001, 34, 1229-1242.	2.1	156
154	Reconstruction of blood flow patterns in a human carotid bifurcation: A combined CFD and MRI study. Journal of Magnetic Resonance Imaging, 2000, 11, 299-311.	3.4	147
155	Blood flow and vessel mechanics in a physiologically realistic model of a human carotid arterial bifurcation. Journal of Biomechanics, 2000, 33, 975-984.	2.1	253
156	Reconstruction of blood flow patterns in a human carotid bifurcation: A combined CFD and MRI study. Journal of Magnetic Resonance Imaging, 2000, 11, 299.	3.4	12
157	Reconstruction of blood flow patterns in human arteries. Proceedings of the Institution of Mechanical Engineers, Part H: Journal of Engineering in Medicine, 1999, 213, 411-421.	1.8	27
158	Flow in carotid bifurcations: effect of the superior thyroid artery. Medical Engineering and Physics, 1999, 21, 207-214.	1.7	25
159	Magnetic resonance image processing and structured grid generation of a human abdominal bifurcation. Computer Methods and Programs in Biomedicine, 1998, 56, 249-259.	4.7	45
160	Fluid-Structure Interaction Simulations of Repaired Type A Aortic Dissection: a Comprehensive Comparison With Rigid Wall Models. Frontiers in Physiology, 0, 13, .	2.8	14